An effective high-order point-collocation numerical approach based on integrated approximants for elliptic differential equations

N. Mai-Duy and T. Tran-Cong*

Computational Engineering and Science Research Centre (CESRC)

Faculty of Engineering and Surveying

The University of Southern Queensland, Toowoomba, QLD 4350, Australia

Submitted to *Applied Mathematical Modeling Research Trends*,

04-Jun-2007

*Corresponding author: E-mail trancong@usq.edu.au, Telephone +61 7 4631 2539, Fax +61 7 4631 2526

Abstract: This chapter presents the basic features of high-order integral collocation techniques and demonstrates their application to engineering problems. Emphasis is placed on the advantage of the integral collocation approach over the conventional differential approach in the treatment of multiple boundary conditions, complex geometries and domain decompositions.

Keywords: Radial basis functions, Chebyshev polynomials, Integral collocation formulation, Multiple boundary conditions, Complex geometries, Domain decompositions.

1 Introduction

Physical phenomena are usually modelled in terms of ordinary differential equations/partial differential equations (ODEs/PDEs). The DE can only rarely be solved in an exact manner. As a result, one must resort to numerical techniques to obtain approximate solutions of the DE. The aim of numerical techniques is to reduce the differential system to an equivalent set of algebraic equations where a solution becomes obtainable. To achieve that, the field variable and the DE need to be discretized, relying on the assumption that any continuous quantity can be approximated by a set of continuous functions.

The governing equation can be represented in a strong, weak or inverse form. The strong form, which is associated with point-collocation techniques such as finite-difference [1] and pseudospectral [2] methods, does not require the integration of the DE. The continuous domain is simply replaced by a set of discrete points. The point-based solution is found using the concept of zero-value of error at certain points over the domain. On the hand, the weak and inverse forms, which are associated with element-based techniques such as finite-element [3] and boundary-element [4]

methods, involve volume and boundary integrals, respectively. The problem domain or its boundary is divided into a set of small elements. The element-based solution is determined using the concept of distribution of error within the domain or along the boundary. Each form has some advantages over the others for certain classes of problems. The weak and inverse forms possess a smoothing capability, while the strong form features a mesh-free property.

In a "differential" numerical technique, the field variable approximation is based on a set of known basis functions with corresponding unknown coefficients. Expressions for its derivatives are then obtained through differentiation. Approximation schemes can be classified into two categories: low order and high order. Each category has its own strengths and weaknesses. The former is straightforward to use. However, its relative low accuracy requires a very fine structure, which could lead to numerical difficulty, to represent accurately the complex solution. For the latter, coarse meshes/grids are usually sufficient for most accuracy requirements. However, high-order approximation schemes should be used with great care. For instant, the use of Lagrange polynomials of high order has a tendency to give results that are oscillatory between data values. Any small level of noise in the interpolating function will be badly magnified through differentiation, causing much larger errors for its derivative representations.

This chapter reviews a high-order point-collocation numerical approach for elliptic DEs based on integrated approximants, and associated results recently discussed in several works, including for example [5-32]. In contrast with the differential approach described above, Mai-Duy and Tran-Cong [5,8] proposed an integral procedure, where the starting points of the approximation process are the highest derivatives of the field variable in the given DE. Lower derivatives, and eventually the variable itself, are symbolically obtained by integration. These integration processes give rise to arbitrary constants that serve as additional expansion coefficients, and

therefore facilitate the employment of some extra equations. It is shown that this feature provides an effective way to handle well-known difficult issues associated with the differential collocation approach such as [14,15,20,21,27,28,30-32]

- the implementation of multiple boundary conditions,
- the description of non-rectangular boundaries in a Cartesian grid, and
- the imposition of higher-order continuity of the approximate solution across subdomain interfaces.

In addition, the use of integration also improves the quality of the approximation of derivative functions as well as the stability of a numerical solution owing to its smoothness property [5-13,16-19,22-26,29].

In this chapter, the integral collocation approach is implemented with radial basis functions and Chebyshev polynomials. It is noted that other types of basis functions can also be applied. For example, an integrated Sinc function approximation method has recently been reported by Li and Wu [24]. An attractive feature of the present high-order integral collocation techniques is that the preprocessing is simple. The problem domain of regular/irregular shape is discretized by using a uniform Cartesian grid for radial basis functions and a tensor product grid formed by Gauss-Lobatto points for Chebyshev polynomials. The approximate expressions representing the field variable and its derivatives over the domain are constructed through one-dimensional integrated approximants along grid lines. Superior accuracy and convergence of integral collocation techniques over differential collocation techniques are demonstrated with the solution of differential problems governed by second- and fourth-order elliptic equations and defined in rectangular and non-rectangular domains.

The remainder of the chapter is organized as follows. Sections 2 and 3 give brief reviews of high-order approximants and collocation methods, respectively. Advantages of the integral collocation approach are presented in Section 4. Section 5 demonstrates its application to engineering problems including structural analysis and fluid flow problems. Section 6 concludes the chapter.

2 High-order approximants

2.1 Radial basis function networks (RBFNs)

RBFNs are known as a universal approximator. The RBFN allows the conversion of a function to be approximated from a low-dimension space to a high-dimension space in which the function is expressed as a weighted linear combination of RBFs [33]

$$f(x) = \sum_{i=1}^{m} w_i g_i(x), \tag{1}$$

where $\{g_i(x)\}_{i=1}^{m}$ the set of RBFs, and $\{w_i\}_{i=1}^{m}$ the set of weights to be found.

According to Micchelli's theorem, there is a large class of RBFs, e.g., multiquadrics, inverse multiquadrics and Gaussian functions, whose interpolation matrices obtained from (1) are always invertible provided that the data points are distinct. This is all that is required for non-singularity of interpolation matrices, whatever the number of data points and the dimension of problem [34]. It has been proved that RBFNs are capable of representing any continuous function to a prescribed degree of accuracy in the L_p norm, $p \in [1, \infty]$ [35]. On the other hand, according to the Cover theorem, the higher the number of RBFs used, the more accurate the approximation will be [36], indicating the property of "mesh convergence" of RBFNs. These important theorems can be seen to provide the basis for the design of RBFNs for the solution

of ODEs/PDEs.

It has generally been accepted that, among RBFNs, the multiquadric (MQ) scheme tends to result in the most accurate approximation. The present integral approach implements the MQ function whose form is

$$g_i(x) = \sqrt{(x - c_i)^2 + a_i^2}, \tag{2}$$

where c_i and a_i are the centre and the width of the ith basis function. The RBF widths are known to strongly affect the performance of RBFNs. However, there is still a lack of mathematical theories for specifying their optimal values. For all numerical examples taken here, the RBF widths are simply chosen as the grid spacing.

2.2 Truncated Chebyshev series expansions (CSEs)

An approximate function f is sought in the truncated Chebyshev series form [2]

$$f(x) = \sum_{k=0}^{N} a_k T_k(x), \tag{3}$$

where $\{a_k\}_{k=0}^{N}$ the set of expansion coefficients and $\{T_k\}_{k=0}^{N}$ the set of Chebyshev polynomials of the first kind that are defined by

$$T_k(x) = \cos(k \arccos(x)), \tag{4}$$

in which $-1 \leq x \leq 1$. The polynomial $T_k(x)$ can be expanded in power series as

$$T_0(x) = 1 \tag{5}$$

$$T_k(x) = \frac{k}{2} \sum_{m=0}^{[k/2]} (-1)^m \frac{2^{k-2m}(k-m-1)!}{m!(k-2m)!} x^{k-2m}, \quad k > 0 \tag{6}$$

where $[k/2]$ is the integer part of $k/2$.

The Chebyshev polynomials are orthogonal

$$\int_{-1}^{1} T_k(x) T_l(x) w(x) dx = \frac{\pi}{2} c_k \delta_{kl}, \tag{7}$$

where $w(x) = \sqrt{1-x^2}$ is the Chebyshev weight function, $c_k = 1$ for $k \geq 1$ and $c_k = 2$ for $k = 0$, and δ_{kl} the Kronecker delta.

At the Gauss-Lobatto points $x_i = \cos i\pi/N,\ i = 0, .., N$, which are widely used in collocation methods, the coefficients a_k are obtained in an explicit form

$$a_k = \frac{2}{N\bar{c}_k} \sum_{i=0}^{N} \frac{T_k(x_i)}{\bar{c}_i} u_i, \quad k = 0, 1, \cdots, N, \tag{8}$$

where $\bar{c}_k = 1$ for $1 \leq k \leq N-1$ and $\bar{c}_k = 2$ for $k = \{0, N\}$.

For smooth problems, the Chebyshev approximation scheme exhibits an exponential rate of convergence as the value of N is increased.

3 Methods of collocation

Let Ω be a bounded region and $\partial\Omega$ be the boundary of Ω. Consider the differential problem that consists of an elliptic DE

$$\mathcal{L}u = b, \tag{9}$$

and a set of prescribed values along $\partial\Omega$, where $\mathcal{L}$ is some differential operator, b a given function and u the field variable.

Collocation methods are seen to be the simplest way to discretize the DE. It consists of two main steps. First, the solution u and its derivatives are approximated by finite sums of smooth functions that are linearly independent. Then, the coefficients associated with the basis functions are determined by forcing the approximate solution to satisfy the DE and the boundary conditions at certain points (collocation points). The choice of functions and distribution of collocation points strongly affect the accuracy of the solution.

This chapter is concerned with two types of very smooth basis functions, namely radial basis functions ($\varphi \equiv g$) and Chebyshev polynomials ($\varphi \equiv T$), that are described above. In the remainder of the chapter, for consistency of notation between the two approximation schemes, the subscripts used in CSEs will also start with 1.

3.1 Conventional differential formulation

RBFNs/CSEs are employed to represent the variable u, followed by successive differentiations to obtain approximate expressions for its derivatives

$$u(x) = \sum_{i=1}^{m} \alpha_i \varphi_i(x) = \sum_{i=1}^{m} \alpha_i D_i^{(0)}(x), \tag{10}$$

$$\frac{du(x)}{dx} = \sum_{k=1}^{m} \alpha_i D_i^{(1)}(x), \tag{11}$$

$$\cdots \quad \cdots \qquad \cdots \qquad \cdots \qquad \cdots$$

$$\frac{d^p u(x)}{dx^p} = \sum_{k=1}^{m} \alpha_i D_i^{(p)}(x), \tag{12}$$

where $D_i^{(1)}(x) = dD_i^{(0)}(x)/dx, \cdots, D_i^{(p)}(x) = dD_i^{(p-1)}(x)dx$.

It has been proved that there is a reduction in convergence rate for derivative functions and this reduction is an increasing function of derivative order [37,38].

3.2 Present integral formulation

RBFNs/CSEs are employed to represent the highest-order derivatives of the variable u in the given DE, followed by successive integrations to obtain approximate

expressions for its lower-order derivatives and the variable itself

$$\frac{d^p u(x)}{dx^p} = \sum_{i=1}^{m} \alpha_i \varphi_i(x) = \sum_{i=1}^{m} \alpha_i I_i^{(p)}(x), \tag{13}$$

$$\frac{d^{p-1} u(x)}{dx^{p-1}} = \sum_{k=1}^{m} \alpha_i I_i^{(p-1)}(x) + c_1, \tag{14}$$

$$\frac{d^{p-2} u(x)}{dx^{p-2}} = \sum_{k=1}^{m} \alpha_i I_i^{(p-2)}(x) + c_1 x + c_2, \tag{15}$$

$$\cdots \quad \cdots \qquad \cdots \qquad \cdots \qquad \cdots$$

$$\frac{du(x)}{dx} = \sum_{k=1}^{m} \alpha_i I_i^{(1)}(x) + c_1 \frac{x^{p-2}}{(p-2)!} + c_2 \frac{x^{p-3}}{(p-3)!} + \cdots + c_{p-2} x + c_{p-1}, \tag{16}$$

$$u(x) = \sum_{k=1}^{m} \alpha_i I_i^{(0)}(x) + c_1 \frac{x^{p-1}}{(p-1)!} + c_2 \frac{x^{p-2}}{(p-2)!} + \cdots + c_{p-1} x + c_p, \tag{17}$$

where $I_i^{(p-1)}(x) = \int I_i^{(p)}(x)dx,\ I_i^{(p-2)}(x) = \int I_i^{(p-1)}(x)dx, \cdots, I_i^{(0)}(x) = \int I_i^{(1)}(x)dx$, and $c_1, c_2, \cdots, c_p$ are integration constants. The integral approximation scheme is said to be of pth-order, denoted by ICSE-p or IRBFN-p, if the pth-order derivative is taken as the staring point. The differential approximation scheme can be considered as a special case of the integral approximation scheme by setting the value of p to zero.

The evaluation of (13)-(17) at a set of collocation points $\{x_i\}_{i=1}^m$ leads to

$$\widehat{\frac{d^p u}{dx^p}} = \widehat{\mathcal{I}}_{[p]}^{(p)} \widehat{s}, \tag{18}$$

$$\widehat{\frac{d^{p-1} u}{dx^{p-1}}} = \widehat{\mathcal{I}}_{[p]}^{(p-1)} \widehat{s}, \tag{19}$$

$$\cdots\cdots\cdots$$

$$\widehat{\frac{du}{dx}} = \widehat{\mathcal{I}}_{[p]}^{(1)} \widehat{s}, \tag{20}$$

$$u = \widehat{\mathcal{I}}_{[p]}^{(0)} \widehat{s}, \tag{21}$$

where subscript $[.]$ and superscript $(.)$ are used to indicate the orders of ICSE/IRBFN

and derivative function, respectively,

$$\widehat{s} = (\alpha_1, \alpha_2, \cdots, \alpha_m, c_1, c_2, \cdots, c_p)^T,$$

$$\widehat{\mathcal{I}}_{[p]}^{(p)} = \begin{bmatrix} I_1^{(p)}(x_1), & I_2^{(p)}(x_1), & \cdots, & I_m^{(p)}(x_1), & 0, & 0, & \cdots, & 0, & 0 \\ I_1^{(p)}(x_2), & I_2^{(p)}(x_2), & \cdots, & I_m^{(p)}(x_2), & 0, & 0, & \cdots, & 0, & 0 \\ \cdots & \cdots & \cdots & \cdots & \cdots & \cdots & \cdots & \cdots & \cdots \\ I_1^{(p)}(x_m), & I_2^{(p)}(x_m), & \cdots, & I_m^{(p)}(x_m), & 0, & 0, & \cdots, & 0, & 0 \end{bmatrix},$$

$$\widehat{\mathcal{I}}_{[p]}^{(p-1)} = \begin{bmatrix} I_1^{(p-1)}(x_1), & I_2^{(p-1)}(x_1), & \cdots, & I_m^{(p-1)}(x_1), & 1, & 0, & \cdots, & 0, & 0 \\ I_1^{(p-1)}(x_2), & I_2^{(p-1)}(x_2), & \cdots, & I_m^{(p-1)}(x_2), & 1, & 0, & \cdots, & 0, & 0 \\ \cdots & \cdots & \cdots & \cdots & \cdots & \cdots & \cdots & \cdots & \cdots \\ I_1^{(p-1)}(x_m), & I_2^{(p-1)}(x_m), & \cdots, & I_m^{(p-1)}(x_m), & 1, & 0, & \cdots, & 0, & 0 \end{bmatrix},$$

$\cdots\cdots$, and

$$\widehat{\mathcal{I}}_{[p]}^{(0)} = \begin{bmatrix} I_1^{(0)}(x_1), & I_2^{(0)}(x_1), & \cdots, & I_m^{(0)}(x_1), & \frac{x_1^{p-1}}{(p-1)!}, & \frac{x_1^{p-2}}{(p-2)!}, & \cdots, & x_1, & 1 \\ I_1^{(0)}(x_2), & I_2^{(0)}(x_2), & \cdots, & I_m^{(0)}(x_2), & \frac{x_2^{p-1}}{(p-1)!}, & \frac{x_2^{p-2}}{(p-2)!}, & \cdots, & x_2, & 1 \\ \cdots & \cdots & \cdots & \cdots & \cdots & \cdots & \cdots & \cdots & \cdots \\ I_1^{(0)}(x_m), & I_2^{(0)}(x_m), & \cdots, & I_m^{(0)}(x_m), & \frac{x_m^{p-1}}{(p-1)!}, & \frac{x_m^{p-2}}{(p-2)!}, & \cdots, & x_m, & 1 \end{bmatrix}.$$

The use of integrated basis functions is expected to overcome the problem of reduction of convergence rate caused by differentiation. Numerical studies on second-order differential problems [5,18,19,29] have indicated that the integral approach produces more accurate results than the differential one. This has recently been theoretically examined with RBFs by Sarra [22], which show the superiority in accuracy of the antiderivative approach.

Another important point here is that additional coefficients (integration constants) can be utilized to handle "extra constraints" related to boundary conditions and geometries. Details are presented in next section.

4 Advantages of the integral collocation approach

4.1 Treatment of multiple boundary conditions

For simplicity, consider the approximation of the solution of the biharmonic equation

$$\frac{\partial^4 u}{\partial x^4} + 2\frac{\partial^4 u}{\partial x^2 \partial y^2} + \frac{\partial^4 u}{\partial y^4} = b(x, y), \tag{22}$$

in a rectangular domain with double boundary conditions u and $\partial u/\partial n$.

For the differential collocation approach, there is normally one equation employed at a point. Boundary conditions for second-order equations (single boundary values) can thus be accommodated in a straightforward manner. However, for higher-order equations, the solution is required to satisfy more than one prescribed value at a boundary point. A number of techniques have been developed for handling multiple boundary conditions, including (i) the node-reduction technique (reducing the number of collocation points used for collocating the governing equation), (ii) the fictitious-point technique (using fictitious points as additional unknowns), and (iii) the imposed-kernel technique (modifying the basis functions to incorporate boundary conditions). In contrast, the integral collocation approach has the ability to deal with multiple boundary conditions in a natural way. The presence of integration constants allows the use of more than one equation at certain points. Such extra equations can be utilized for the purpose of imposing the value of the normal derivative and the governing equation at boundary points.

In currently used notations, $\widehat{\ }$ and $\widetilde{\ }$ denote vectors/matrices that are associated with a grid line (one-dimensional domain) and the whole set of grid lines (two-dimensional domain), respectively.

The integral collocation schemes of fourth order are employed here to discretize derivative terms in the biharmonic equation. It is more convenient to work in the physical space than in the spectral space. Consider a horizontal grid line. The presence of four integration constants in the integral formulation allows one to add four extra equations to the conversion system. These equations can be chosen to represent the value of the normal derivative and the governing equation at both ends of the line. The conversion process of the spectral space into the physical space is constructed by

$$\begin{pmatrix} \widehat{u} \\ \widehat{v} \end{pmatrix} = \begin{bmatrix} \widehat{\mathcal{I}}^{(0)}_{[4]} \\ \widehat{\mathcal{B}} \end{bmatrix} \begin{pmatrix} \widehat{\alpha} \\ \widehat{c} \end{pmatrix} = \widehat{\mathcal{C}} \begin{pmatrix} \widehat{\alpha} \\ \widehat{c} \end{pmatrix}, \tag{23}$$

where $\widehat{\mathcal{I}}^{(0)}_{[4]}$ is defined as before,

$$\widehat{\alpha} = \begin{pmatrix} \alpha_1 \\ \alpha_2 \\ \cdots \\ \alpha_{n_x} \end{pmatrix}, \qquad \widehat{c} = \begin{pmatrix} c_1 \\ c_2 \\ c_3 \\ c_4 \end{pmatrix}, \qquad \widehat{u} = \begin{pmatrix} u_1 \\ u_2 \\ \cdots \\ u_{n_x} \end{pmatrix},$$

$$\widehat{v} = \begin{pmatrix} \frac{\partial u}{\partial x}(x_1) \\ \frac{\partial u}{\partial x}(x_{n_x}) \\ b(x_1) - 2\frac{\partial^4 u}{\partial x^2 y^2}(x_1) - \frac{\partial^4 u}{\partial y^4}(x_1) \\ b(x_{n_x}) - 2\frac{\partial^4 u}{\partial x^2 y^2}(x_{n_x}) - \frac{\partial^4 u}{\partial y^4}(x_{n_x}) \end{pmatrix},$$

$$\widehat{\mathcal{B}} = \begin{bmatrix} I^{(1)}_1(x_1) & \cdots & I^{(1)}_{n_x}(x_1) & x_1^2/2 & x_1 & 1 & 0 \\ I^{(1)}_1(x_{n_x}) & \cdots & I^{(1)}_{n_x}(x_{n_x}) & x_{n_x}^2/2 & x_{n_x} & 1 & 0 \\ I^{(4)}_1(x_1) & \cdots & I^{(4)}_{n_x}(x_1) & 0 & 0 & 0 & 0 \\ I^{(4)}_1(x_{n_x}) & \cdots & I^{(4)}_{n_x}(x_{n_x}) & 0 & 0 & 0 & 0 \end{bmatrix}_{[4]},$$

and n_x is the number of collocation points on the grid line ($n_x = m$).

Solving (23) yields

$$\begin{pmatrix} \widehat{\alpha} \\ \widehat{c} \end{pmatrix} = \widehat{\mathcal{C}}^{-1} \begin{pmatrix} \widehat{u} \\ \widehat{v} \end{pmatrix}. \tag{24}$$

Taking (24) into account, the values of derivatives of the variable u at a point on the line are computed by

$$\frac{\partial^4 u(x)}{\partial x^4} = \left(I_1^{(4)}(x), I_2^{(4)}(x), \cdots, I_{n_x}^{(4)}(x), 0, 0, 0, 0\right) \widehat{\mathcal{C}}^{-1} \begin{pmatrix} \widehat{u} \\ \widehat{v} \end{pmatrix}, \tag{25}$$

$$\frac{\partial^3 u(x)}{\partial x^3} = \left(I_1^{(3)}(x), I_2^{(3)}(x), \cdots, I_{n_x}^{(3)}(x), 1, 0, 0, 0\right) \widehat{\mathcal{C}}^{-1} \begin{pmatrix} \widehat{u} \\ \widehat{v} \end{pmatrix}, \tag{26}$$

$$\frac{\partial^2 u(x)}{\partial x^2} = \left(I_1^{(2)}(x), I_2^{(2)}(x), \cdots, I_{n_x}^{(2)}(x), x, 1, 0, 0\right) \widehat{\mathcal{C}}^{-1} \begin{pmatrix} \widehat{u} \\ \widehat{v} \end{pmatrix}, \tag{27}$$

$$\frac{\partial u(x)}{\partial x} = \left(I_1^{(1)}(x), I_2^{(1)}(x), \cdots, I_{n_x}^{(1)}(x), \frac{x^2}{2}, x, 1, 0\right) \widehat{\mathcal{C}}^{-1} \begin{pmatrix} \widehat{u} \\ \widehat{v} \end{pmatrix}. \tag{28}$$

The evaluation of (25)-(28) at the grid points leads to

$$\widehat{\frac{\partial^i u}{\partial x^i}} = \widehat{\mathcal{D}}_{ix} \begin{pmatrix} \widehat{u} \\ \widehat{v} \end{pmatrix}, \qquad i = \{1, 2, 3, 4\}, \tag{29}$$

where $\widehat{\frac{\partial^i u}{\partial x^i}} = \left(\frac{\partial^i u_1}{\partial x^i}, \frac{\partial^i u_2}{\partial x^i}, \cdots, \frac{\partial^i u_{n_x}}{\partial x^i}\right)^T$ and $\widehat{\mathcal{D}}_{ix}$ is the $n_x \times (n_x + 4)$ matrix of known quantities related to geometry and discretization.

Expression (29) can be rewritten as $\widehat{\frac{\partial^i u}{\partial x^i}} = \widehat{\mathcal{D}}_{ix}^{\dagger} \widehat{u} + \widehat{\mathcal{D}}_{ix}^{\ddagger} \widehat{v}$, where $\widehat{\mathcal{D}}_{ix}^{\dagger}$ and $\widehat{\mathcal{D}}_{ix}^{\ddagger}$ are matrices that are formed by the first n_x columns and the last four columns of the matrix $\widehat{\mathcal{D}}_{ix}$, respectively. The extra information vector $\widehat{v}$ (components v_3 and v_4) contains some unknown values—the mixed partial derivative $\partial^4 u / \partial x^2 \partial y^2$ at the two boundary points. Fortunately, these unknown values can be replaced with linear

combinations of nodal values of the variable u (the detailed expression of $\partial^4 u/\partial x^2 \partial y^2$ will be given later on). As a result, one can express (29) in terms of nodal variable values only. The values of the ith-order derivative of u with respect to y at the collocation points along a vertical line will be obtained in the same way.

The approximations for derivatives over 2D grids can be conveniently constructed by means of Kronecker tensor products. Assuming that the grid points are numbered from bottom to top and from left to right, the values of derivatives of u at the grid points are computed by

$$\widetilde{\frac{\partial^i u}{\partial x^i}} = \left(\widehat{\mathcal{D}}_{ix} \otimes \widehat{\mathcal{I}}_y\right) \widetilde{u} + \widetilde{k}_{ix}, \qquad \widetilde{\frac{\partial^i u}{\partial y^i}} = \left(\widehat{\mathcal{I}}_x \otimes \widehat{\mathcal{D}}_{iy}\right) \widetilde{u} + \widetilde{k}_{iy}, \tag{30}$$

where $\otimes$ is the Kronecker tensor product, $\widehat{\mathcal{I}}_x$ and $\widehat{\mathcal{I}}_y$ are the identity matrices of sizes $n_x \times n_x$ and $n_y \times n_y$, respectively, $\widetilde{k}_{ix}$ and $\widetilde{k}_{iy}$ are the vectors of known quantities related to boundary conditions, and $\widetilde{u} = \left(u_1, u_2, \cdots, u_{n_x n_y}\right)^T$.

The integral collocation approach employs the following relation to calculate the mixed fourth-order derivative

$$\frac{\partial^4 u}{\partial^2 x \partial^2 y} = \frac{1}{2}\left[\frac{\partial^2}{\partial x^2}\left(\frac{\partial^2 u}{\partial y^2}\right) + \frac{\partial^2}{\partial y^2}\left(\frac{\partial^2 u}{\partial x^2}\right)\right]. \tag{31}$$

This expression reduces the computation of fourth-order mixed derivatives to that of second-order pure derivatives for which IRBFNs/ICSEs involve integration with respect to x or y only. Integral schemes of second order are used here to approximate these second-order derivatives with the extra information being the values of the corresponding first-order derivatives at the boundary points.

It can be seen that the integrated approximants contain information about boundary conditions. As a result, it remains only to force these approximations to satisfy the governing equation. Collocating the PDE (22) at the interior points leads to a

determinate system of algebraic equations for the unknown vector of nodal interior values of the variable u.

The integral and differential collocation approaches are applied to solve the following test problem

$$b(x, y) = 4 \sin(\pi x) \sin(\pi y), \tag{32}$$

$$u_e = \frac{1}{\pi^4} \sin(\pi x) \sin(\pi y), \tag{33}$$

$$\Omega \equiv [-1, -1] \times [1, 1], \tag{34}$$

where u_e denotes the exact solution of the problem.

Results concerning the discrete relative L_2 error of the solution u, $N_e(u)$, and the condition number of the system matrix, cond($\mathcal{A}$), obtained by the two approaches are presented in Tables 1 and 2 for CSEs and RBFNs, respectively. For the differential approach, double boundary conditions are implemented here using the node-reduction technique. The PDE is collocated at the $(n_x - 4)(n_y - 4)$ interior points $(x_i, y_j),\ i = (3, 4, \cdots, n_x - 2),\ j = (3, 4, \cdots, n_y - 2)$. Along the two vertical lines, boundary conditions $\partial u/\partial n$ are imposed at the $2(n_y - 2)$ nodal points; while along the two horizontal lines, they are imposed at the $2(n_x - 4)$ nodal points. The discretized boundaries do not include the four corners of the domain. This leads to a square set of algebraic equations. Like conventional RBF techniques, the present differential RBF collocation technique approximates a solution in terms of network weights. For both cases (RBFNs and CSEs), the performance of the integral approach is superior to that of the differential approach.

4.2 Description of non-rectangular boundaries in a Cartesian grid

The application of finite-difference and pseudospectral methods to irregularly-shaped domains requires coordinate transformations. First, a physical domain of complex geometry is converted into a computational domain of regular geometry. Then, an equivalent problem is derived by transforming the governing equation into the computational coordinate system. The relationships between the two coordinates systems are usually given in the form of PDEs. Such a procedure is quite cumbersome. In contrast, the complicated coordinate transformations are avoided in Cartesian-grid methods, which are the concern of this section. They are implemented with ICSEs and IRBFNs. The incorporation of prescribed values on immersed boundaries are conducted in a way that does not adversely affect the accuracy of the numerical method. There are some differences in boundary treatment between the two present approximation schemes, which are presented through the second-order Dirichlet differential problem governed by

$$\frac{\partial^2 u}{\partial x^2} + \frac{\partial^2 u}{\partial y^2} = b(x, y), \tag{35}$$

in a circular domain Ω with a unit radius.

4.2.1 ICSEs

Figure 1 shows an extension of Ω to the reference square that is discretized using a tensor product grid formed by Gauss-Lobatto points. It can be seen that the grid points do not generally lie on the boundary of the domain. Integration constants are utilized here to include information on the boundary in the Chebyshev approximations.

Lines aa' and bb' in Figure 1 present typical cases for the approximation of $\partial u/\partial x$ and $\partial^2 u/\partial x^2$.

4.2.2 Case 1 - Line aa':

Along this line, there are two boundary points x_{b1} and x_{b2}. Assume that they are not grid points. The ICSE-2 scheme can be employed to impose the two boundary conditions. The conversion of the spectral space into the physical space is based on the following system

$$\begin{pmatrix} \widehat{u} \\ u_{b1} \\ u_{b2} \end{pmatrix} = \begin{bmatrix} \widehat{\mathcal{I}}^{(0)}_{[2]} \\ \widehat{\mathcal{B}} \end{bmatrix} \begin{pmatrix} \widehat{\alpha} \\ c_1 \\ c_2 \end{pmatrix} = \widehat{C} \begin{pmatrix} \widehat{\alpha} \\ c_1 \\ c_2 \end{pmatrix}, \tag{36}$$

where $\widehat{\mathcal{I}}^{(0)}_{[2]}$ is as before,

$$\widehat{\alpha} = (\alpha_1, \alpha_2, \cdots, \alpha_{n_x})^T, \tag{37}$$

$$\widehat{u} = (u_1, u_2, \cdots, u_{n_x})^T, \tag{38}$$

$$\widehat{\mathcal{B}} = \begin{bmatrix} I^{(0)}_1(x_{b1}), & I^{(0)}_2(x_{b1}), & \cdots, & I^{(0)}_{n_x}(x_{b1}), & x_{b1}, & 1 \\ I^{(0)}_1(x_{b2}), & I^{(0)}_2(x_{b2}), & \cdots, & I^{(0)}_{n_x}(x_{b2}), & x_{b2}, & 1 \end{bmatrix}_{[2]},$$

and n_x is the number of collocation points on the grid line.

Solving (36) yields

$$\begin{pmatrix} \widehat{\alpha} \\ c_1 \\ c_2 \end{pmatrix} = \widehat{\mathcal{C}}^{-1} \begin{pmatrix} \widehat{u} \\ u_{b1} \\ u_{b2} \end{pmatrix}. \tag{39}$$

The values of $\partial u/\partial x$ and $\partial^2 u/\partial x^2$ at the grid points are then computed by

$$\widehat{\frac{\partial u}{\partial x}} = \widehat{\mathcal{I}}^{(1)}_{[2]} \widehat{\mathcal{C}}^{-1} \begin{pmatrix} \widehat{u} \\ u_{b1} \\ u_{b2} \end{pmatrix}, \tag{40}$$

$$\widehat{\frac{\partial^2 u}{\partial x^2}} = \widehat{\mathcal{I}}^{(2)}_{[2]} \widehat{\mathcal{C}}^{-1} \begin{pmatrix} \widehat{u} \\ u_{b1} \\ u_{b2} \end{pmatrix}. \tag{41}$$

4.2.3 Case 2 - Line bb':

A number of schemes can be applied here. In the following, two typical schemes are presented.

If the contact point x_b is not a grid node, one can use ICSE-1

$$\begin{pmatrix} \widehat{u} \\ u_b \end{pmatrix} = \begin{bmatrix} \widehat{\mathcal{I}}^{(0)}_{[1]} \\ \widehat{\mathcal{B}} \end{bmatrix} \begin{pmatrix} \widehat{\alpha} \\ c_1 \end{pmatrix}, \tag{42}$$

where

$$\widehat{\mathcal{B}} = \begin{bmatrix} I^{(0)}_1(x_b), & I^{(0)}_2(x_b), & \cdots, & I^{(0)}_{n_x}(x_b), & 1 \end{bmatrix}_{[1]}.$$

If the contact point is also a grid node, one can employ ICSE-0 or ICSE-2. For the latter, the conversion system is given by

$$\begin{pmatrix} \widehat{u} \\ \frac{\partial u_b}{\partial x} \\ \frac{\partial^2 u_b}{\partial x^2} \end{pmatrix} = \begin{bmatrix} \widehat{\mathcal{I}}^{(0)}_{[2]} \\ \widehat{\mathcal{B}} \end{bmatrix} \begin{pmatrix} \widehat{\alpha} \\ c_1 \\ c_2 \end{pmatrix}, \tag{43}$$

where

$$\widehat{\mathcal{B}} = \begin{bmatrix} I_1^{(1)}(x_b), & I_2^{(1)}(x_b), & \cdots, & I_{n_x}^{(1)}(x_b), & 1, & 0 \\ I_1^{(2)}(x_b), & I_2^{(2)}(x_b), & \cdots, & I_{n_x}^{(2)}(x_b), & 0, & 0 \end{bmatrix}_{[2]}.$$

In (43), $\partial u_b/\partial x$ and $\partial^2 u_b/\partial x^2$ are known values, which are derived from using boundary conditions.

The remaining steps for obtaining the Chebyshev approximations of $\partial u/\partial x$ and $\partial^2 u/\partial x^2$ are similar to Case 1 and therefore omitted here for brevity.

The values of $\partial u/\partial y$ and $\partial^2 u/\partial y^2$ at the grid points along vertical lines can be computed in a similar fashion.

The Chebyshev approximations of derivatives at a grid point are expressed in terms of the nodal values of u along the grid lines that goes through that point. It should be emphasized that they already contain information about the boundary of Ω (i.e. locations and boundary values). As with finite-difference, finite-element and boundary-element techniques, one will gather these approximations together to form the global matrices for the discretization of the PDE. This task is relatively simple since the grid used here is regular. By collocating the governing equation at the grid points and then deleting rows corresponding to points that lie on the boundary, a square system of algebraic equations is obtained, which is solved for the approximate solution.

4.2.4 IRBFNs

Unlike ICSEs, IRBFNs have the capability to handle unstructured points with accuracy. The problem domain is embedded in a Cartesian grid with a grid spacing h. Grid points outside the domain (external points) together with internal points that fall very close–within a distance of $h/8$–to the boundary are removed. The

remaining grid points are taken to be the interior nodes (Figure 2). The boundary nodes consists of the grid points that lie on the boundaries, and points that are generated by the intersection of the grid lines with the boundaries.

The one-dimensional IRBFN schemes are employed to discretize the solution and its relevant derivatives along grid lines. As presented earlier, an IRBFN-p scheme permits the approximation of a function and its derivatives of orders up to p. To use integrated basis functions only, one needs to employ IRBFNs of at least second order. A line in the grid contains two sets of points (Figure 3). The first set consists of the interior points that are also the grid nodes (regular nodes). The values of the variable u at the interior points are unknown. The second set is formed from the boundary nodes that do not generally coincide with the grid nodes (irregular nodes). At the boundary nodes, the values of the variable u are given. Unlike finite-difference and pseudospectral methods, the involvement of irregular points here does not adversely affect the accuracy of the IRBFN scheme.

Consider a horizontal grid line (Figure 3). An important feature of the present IRBFN technique is that, along the grid line, both interior points $\{x_i\}_{i=1}^{q}$ and boundary points $\{x_{bi}\}_{i=1}^{2}$ are taken to be the centres of the network. This work employs IRBFN-2s to discretize the field variable. The conversion system is constructed as follows

$$\begin{pmatrix} \widehat{u} \\ u_{b1} \\ u_{b2} \end{pmatrix} = \begin{bmatrix} \widehat{\mathcal{I}}_{[2]}^{(0)} \\ \widehat{\mathcal{B}} \end{bmatrix} \begin{pmatrix} \widehat{\alpha} \\ c_1 \\ c_2 \end{pmatrix} = \widehat{\mathcal{C}} \begin{pmatrix} \widehat{\alpha} \\ c_1 \\ c_2 \end{pmatrix}, \tag{44}$$

where $\widehat{\mathcal{I}}^{(0)}_{[2]}$ is defined as before,

$$\widehat{u} = (u_1, u_2, \cdots, u_q)^T,$$
$$\widehat{\alpha} = (\alpha_1, \alpha_2, \cdots, \alpha_m)^T,$$
$$\widehat{\mathcal{B}} = \begin{bmatrix} I_1^{(0)}(x_{b1}) & \cdots & I_m^{(0)}(x_{b1}) & x_{b1} & 1 \\ I_1^{(0)}(x_{b2}) & \cdots & I_m^{(0)}(x_{b2}) & x_{b2} & 1 \end{bmatrix}_{[2]},$$

and $m = q + 2$.

The obtained system (44) for the unknown vector of network weights can be solved using the singular value decomposition technique

$$\begin{pmatrix} \widehat{\alpha} \\ c_1 \\ c_2 \end{pmatrix} = \widehat{\mathcal{C}}^{-1} \begin{pmatrix} \widehat{u} \\ u_{b1} \\ u_{b2} \end{pmatrix}. \tag{45}$$

The values of the first and second derivatives of u at the interior points are computed as follows

$$\begin{pmatrix} \frac{\partial u_1}{\partial x} \\ \frac{\partial u_2}{\partial x} \\ \vdots \\ \frac{\partial u_q}{\partial x} \end{pmatrix} = \begin{bmatrix} I_1^{(1)}(x_1) & \cdots & I_m^{(1)}(x_1) & 1 & 0 \\ I_1^{(1)}(x_2) & \cdots & I_m^{(1)}(x_2) & 1 & 0 \\ \cdots & \cdots & \cdots & \cdots & \cdots \\ I_1^{(1)}(x_q) & \cdots & I_m^{(1)}(x_q) & 1 & 0 \end{bmatrix}_{[2]} \widehat{\mathcal{C}}^{-1} \begin{pmatrix} \widehat{u} \\ u_{b1} \\ u_{b2} \end{pmatrix}, \tag{46}$$

and

$$\begin{pmatrix} \frac{\partial^2 u_1}{\partial x^2} \\ \frac{\partial^2 u_2}{\partial x^2} \\ \vdots \\ \frac{\partial^2 u_q}{\partial x^2} \end{pmatrix} = \begin{bmatrix} I_1^{(2)}(x_1) & \cdots & I_m^{(2)}(x_1) & 0 & 0 \\ I_1^{(2)}(x_2) & \cdots & I_m^{(2)}(x_2) & 0 & 0 \\ \cdots & \cdots & \cdots & \cdots & \cdots \\ I_1^{(2)}(x_q) & \cdots & I_m^{(2)}(x_q) & 0 & 0 \end{bmatrix}_{[2]} \widehat{\mathcal{C}}^{-1} \begin{pmatrix} \widehat{u} \\ u_{b1} \\ u_{b2} \end{pmatrix}, \tag{47}$$

or in compact forms

$$\widehat{\frac{\partial u}{\partial x}} = \widehat{\mathcal{D}}_{1x}\widehat{u} + \widehat{k}_{1x}, \tag{48}$$

and

$$\widehat{\frac{\partial^2 u}{\partial x^2}} = \widehat{\mathcal{D}}_{2x}\widehat{u} + \widehat{k}_{2x}, \tag{49}$$

where $\widehat{k}_{1x}$ and $\widehat{k}_{2x}$ are the vectors of known quantities related to boundary conditions.

It can be seen from (48) and (49) that the IRBFN approximations of $\partial u/\partial x$ and $\partial^2 u/\partial x^2$ at the interior points include information about the boundary (locations and boundary values).

The incorporation of the boundary points into the set of centres has several advantages:

- It allows the two sets of centres and collocation points to be the same, i.e. $\{c_i\}_{i=1}^{m} \equiv \left\{\{x_i\}_{i=1}^{q} \cup \{x_{bi}\}_{i=1}^{2}\right\}$. Numerical investigations have indicated that when these two sets coincide, the RBF approximation scheme tends to result in the most accurate numerical solution [5,6].

- It allows the use of IRBFNs with a fixed order (IRBFN-2), regardless of the shape of the domain. In contrast, the order of the ICSE scheme depends on the number of intersections between a grid line and the boundaries.

In the same manner, one can obtain the IRBF expressions for $\partial u/\partial y$ and $\partial^2 u/\partial y^2$ at the interior points along a vertical line.

The "local" IRBF approximations along grid lines will be assembled to build the discrete representation of the PDE. Collocating the governing equation at the interior points results in a square system of algebraic equations, which is solved for the values of u within the spatial domain.

Numerical studies are conducted for the following driving and exact functions

$$b(x,y) = -2\sin(\pi x)\sin(\pi y), \tag{50}$$

$$u_e(x,y) = \frac{1}{\pi^2}\sin(\pi x)\sin(\pi y). \tag{51}$$

Condition numbers of the system matrix and relative L_2 errors of the solution u are shown in Tables 3 and 4 for ICSEs and IRBFNs, respectively. Results indicate that the two techniques preserve their fast rates of convergence with grid refinement. The process of handling irregular geometries here is much simpler than that using coordinate transformations.

4.3 Improvement of continuity order across subdomain interfaces

The use of domain decompositions (DDs) is necessary to handle large-scale domains and complex geometries. The problem domain is partitioned into a set of subdomains that can be overlapped or non-overlapped. An important feature of DDs is that the size of the matrices involved is much smaller than that associated with a single domain. With the recent emergence of parallel computers, the DD methods have become more attractive because they allow the parallel implementation of discretization schemes. However, the main drawback of the DD methods is that they provide a less smooth solution than a single-domain method. Let p be the order of the governing equation. Conventional DD techniques are only able to impose a $C^{(p-1)}$ solution across subdomain interfaces, a situation we seek to improve here.

This chapter is concerned with non-overlapping domain decompositions. It is shown that the integral collocation approach has the capability to force the C^p, instead of the usual C^{p-1}, continuity of the approximate solution across the subdomain

interfaces.

For the sake of simplicity, the basic features of the present DD scheme are described through the following second-order ODE

$$\kappa \frac{d^2u}{dx^2} + \beta \frac{du}{dx} + \gamma u = b(x), \tag{52}$$

defined on the domain $a \leq x \leq b$ and subject to the Dirichlet boundary conditions at both ends: $\bar{u}_a$ and $\bar{u}_b$.

A substructuring method [39] is applied here, which involves two main steps: (i) To find the values of the variable u at the interface points/interior-boundary-points (the interface solution) and (ii) To find the values of the variable u at the interior points in subdomains (the subdomain solution). The present substructuring technique is based on the use of integrated approximants (ICSEs/IRBFNs) to represent approximate solutions in subdomains.

4.3.1 The interface solution

The domain of interest is divided into M subdomains. Each subdomain is discretized using a set of n Gauss-Lobatto points via the following coordinate transformation

$$x^{[j]} = \frac{x_r^{[j]} - x_l^{[j]}}{2}\xi + \frac{x_r^{[j]} + x_l^{[j]}}{2} = \frac{L^{[j]}}{2}\xi + \frac{x_r^{[j]} + x_l^{[j]}}{2}, \tag{53}$$

in which $x_l^{[j]}$ and $x_r^{[j]}$ are the coordinates of the boundary points of a subdomain j, $L^{[j]} = x_r^{[j]} - x_l^{[j]}$, and ξ the Gauss-Lobatto points ($-1 \leq \xi \leq 1$).

The continuity of the solution and its flux leads to the following constraint equations

$$u_n^{[j]} = u_1^{[j+1]}, \tag{54}$$

$$\left(\frac{du}{dx}\right)_n^{[j]} = \left(\frac{du}{dx}\right)_1^{[j+1]}, \tag{55}$$

where $j = \{1, 2, \cdots, M-1\}$.

The present scheme requires the solution u to be continuous, i.e.

$$u_n^{[j]} = u_1^{[j+1]} = \bar{u}_j, \quad j = \{1, 2, \cdots, M-1\}, \tag{56}$$

and its derivatives to be matched at the interfaces. This approach allows an easy implementation (automation) of the computer code.

Consider a subdomain j. Using integrated approximations (13)-(17) with $p = 2$, the governing equation (52) and the boundary conditions can be transformed into

$$\frac{4\kappa}{L^{[j]2}} \sum_{k=1}^{n} \alpha_k^{[j]} I_k^{(2)}(\xi) + \frac{2\beta}{L^{[j]}} \left(\sum_{k=1}^{n} \alpha_k^{[j]} I_k^{(1)}(\xi) + c_1^{[j]} \right)$$
$$+ \gamma \left(\sum_{k=1}^{n} \alpha_k^{[j]} I_k^{(0)}(\xi) + c_1^{[j]} \xi + c_2^{[j]} \right) = b(x^{[j]}(\xi)), \tag{57}$$

$$\sum_{k=1}^{n} \alpha_k^{[j]} I_k^{(0)}(-1) - c_1^{[j]} + c_2^{[j]} = \bar{u}_{j-1}, \tag{58}$$

$$\sum_{k=1}^{n} \alpha_k^{[j]} I_k^{(0)}(+1) + c_1^{[j]} + c_2^{[j]} = \bar{u}_j, \tag{59}$$

where $\bar{u}_{j-1} = \bar{u}_a$ for $j = 1$, $\bar{u}_j = \bar{u}_b$ for $j = M$, and the unknowns are the set of expansion coefficients and integration constants.

The evaluation of (57) at the whole set of Gauss-Lobatto points $\{\xi_i\}_{i=1}^n$ plus the boundary conditions (58)-(59) results in a determinate system of equations of the

form

$$\mathbf{A}^{[j]} \begin{pmatrix} \alpha_1^{[j]} \\ \alpha_2^{[j]} \\ \cdots \\ \alpha_n^{[j]} \\ c_1^{[j]} \\ c_2^{[j]} \end{pmatrix} = \begin{pmatrix} b_1^{[j]} \\ b_2^{[j]} \\ \cdots \\ b_n^{[j]} \\ \bar{u}_{j-1} \\ \bar{u}_j \end{pmatrix}, \tag{60}$$

or

$$\mathbf{A}^{[j]} \widehat{s}^{[j]} = \begin{pmatrix} \widehat{b}^{[j]} \\ \bar{u}_{j-1} \\ \bar{u}_j \end{pmatrix}, \tag{61}$$

where $\mathbf{A}^{[j]}$ is the known matrix of dimension $(n+2) \times (n+2)$. Unlike conventional differential formulations, the governing equation (52) is forced to be satisfied at the two boundary points exactly in (61) (the first and nth rows)

$$\kappa \left(\frac{d^2 u}{dx^2} \right)_1^{[j]} + \beta \left(\frac{du}{dx} \right)_1^{[j]} + \gamma u_1^{[j]} = b_1^{[j]}, \tag{62}$$

$$\kappa \left(\frac{d^2 u}{dx^2} \right)_n^{[j]} + \beta \left(\frac{du}{dx} \right)_n^{[j]} + \gamma u_n^{[j]} = b_n^{[j]}. \tag{63}$$

Solving (61) yields

$$\widehat{s}^{[j]} = \left(\mathbf{A}^{[j]} \right)^{-1} \begin{pmatrix} \widehat{b}^{[j]} \\ \bar{u}_{j-1} \\ \bar{u}_j \end{pmatrix}. \tag{64}$$

As mentioned earlier, the interface unknown vector, namely $(\bar{u}_1, \bar{u}_2, \cdots, \bar{u}_{M-1})^T$, are determined by the imposition of continuity of the first-order normal derivative at

the interfaces

$$\left(\frac{du}{dx}\right)_n^{[1]} = \left(\frac{du}{dx}\right)_1^{[2]}, \tag{65}$$

$$\left(\frac{du}{dx}\right)_n^{[2]} = \left(\frac{du}{dx}\right)_1^{[3]}, \tag{66}$$

$$\cdots \qquad \cdots$$

$$\left(\frac{du}{dx}\right)_n^{[M-1]} = \left(\frac{du}{dx}\right)_1^{[M]}, \tag{67}$$

where

$$\frac{du^{[j]}(x(\xi))}{dx} = \frac{2}{L^{[j]}}\left(\sum_{k=1}^{n}\alpha_k^{[j]} I_k^{(1)}(\xi) + c_1^{[j]} + 0\right) = \frac{2}{L^{[j]}}\left[I_1^{(1)}, I_2^{(1)}, \cdots, I_n^{(1)}, 1, 0\right]\widehat{s}^{[j]}. \tag{68}$$

Substituting (64) into (65)-(67) and then imposing the prescribed boundary conditions $\bar{u}_a$ and $\bar{u}_b$ yield the following square system of equations

$$\mathbf{A}_f \begin{pmatrix} \bar{u}_1 \\ \bar{u}_2 \\ \cdots \\ \bar{u}_{M-1} \end{pmatrix} = \widehat{g}, \tag{69}$$

where $\mathbf{A}_f$ is the known interface matrix of dimension $(M-1)\times(M-1)$, and $\widehat{g}$ the vector of known quantities related to $b(x)$, $\bar{u}_a$ and $\bar{u}_b$.

From (56), (65)-(67), and (62)-(63), it can be seen that the following relations are

imposed at an interface j

$$u_n^{[j]} = u_1^{[j+1]}, \tag{70}$$

$$\left(\frac{du}{dx}\right)_n^{[j]} = \left(\frac{du}{dx}\right)_1^{[j+1]}, \tag{71}$$

$$\kappa \left(\frac{d^2u}{dx^2}\right)_n^{[j]} + \beta \left(\frac{du}{dx}\right)_n^{[j]} + \gamma u_n^{[j]} = b_n^{[j]}, \tag{72}$$

$$\kappa \left(\frac{d^2u}{dx^2}\right)_1^{[j+1]} + \beta \left(\frac{du}{dx}\right)_1^{[j+1]} + \gamma u_1^{[j+1]} = b_1^{[j+1]}. \tag{73}$$

Since $b_n^{[j]} = b_1^{[j+1]}$, (70)-(73) lead to

$$\left(\frac{d^2u}{dx^2}\right)_n^{[j]} = \left(\frac{d^2u}{dx^2}\right)_1^{[j+1]}. \tag{74}$$

Thus, C^p continuity ($p = 2$ in this example) is automatically satisfied in general.

4.3.2 The subdomain solution

Substitutions of the interface values obtained from solving (69) into (64) yield the sets of expansion coefficients and integration constants for subdomains, and hence the solution to the original problem is obtained. It is noted that each subdomain can be analyzed separately, offering an opportunity for parallelization.

Numerical results are presented for the following data

$$\kappa = 1, \quad \beta = 0, \quad \gamma = 0, \tag{75}$$

$$b = -\sin(\pi x), \tag{76}$$

$$u_e = \frac{1}{\pi^2}\sin(\pi x), \tag{77}$$

$$-1 \le x \le 1. \tag{78}$$

The problem domain is decomposed into 5 subdomains of equal length. Each subdomain is discretized using different sets of collocation points. The accuracy of a numerical technique is presented in the form of the relative L_2 norm of the solution u calculated at a test set of 201 uniformly distributed points. Both CSEs and RBFNs are applied here. Parameters used in the differential and integral approaches are exactly the same (e.g. RBF widths are all chosen as grid spacing). Tables 5 and 6 indicate that the DD scheme based on integration performs much better than that based on differentiation.

The present numerical schemes can be extended to solve higher-dimensional problems and higher-order DEs. Similarly, the C^p continuity of the solution over contiguous regions is achieved owing to the satisfaction of the governing equation at the boundary points in each subdomain. The boundary conditions at the interfaces can be chosen to be $\{u, du/dn, ..., d^{p/2-1}u/dn^{p/2-1}\}$, and these unknown values are then determined by the imposition of continuity in the $(p/2), (p/2+1), \cdots, (p-1)$th-order normal derivatives across the interfaces.

5 Some applications of the integral collocation approach

This section presents several applications of the integral collocation approach in the simulation of engineering problems. The first two problems are concerned with structural analysis, while the third one is about the motion of a fluid.

5.1 Free vibration of ring-like structures

The structural element is a ring of rectangular cross-section of constant width and thickness that varies parabolically according to the relation (Figure 4):

$$h(\bar{\theta}) = h(0)\left[-\frac{4}{\pi^2}(r-1)\bar{\theta}^2 + \frac{4}{\pi}(r-1)\bar{\theta} + 1\right] = h(0)f(\bar{\theta}), \tag{79}$$

where $r = h(\pi/2)/h(0)$. The case of normal, in-plane modes of vibration is considered here, where only flexural effects are taken into account and one disregards stretching in the axial direction. Its vibrational behaviour can be modelled by a sixth-order ODE. The problem is simulated with ICSEs. The obtained results are compared with those of the optimized Rayleigh-Ritz method [40] and the differential quadrature technique [41].

5.1.1 A circular ring with supports

Since the structure is symmetric, only half of the domain is considered. Introducing the dimensionless variable $\theta = \bar{\theta}/\pi$, the governing differential equation can be expressed in the form

$$\beta_1 v^{[6]} + \beta_2 v^{[5]} + \beta_3 v^{[4]} + \beta_4 v''' + \beta_5 v'' + \beta_6 v' - \Omega^2\left(fv'' + f'v' - \pi^2 fv\right) = 0, \tag{80}$$

with boundary conditions

$$v(0) = v'(0) = v'''(0) = 0, \quad v(1) = v'(1) = v'''(1) = 0,$$

where $v^{[q]} = d^q v/d\theta^q$, v is the tangential displacement, θ is the dimensionless variable, Ω is the dimensionless frequency, and

$$
\begin{aligned}
&0 \le \theta \le 1,\\
&\beta_1 = \phi/\pi^4, \quad \beta_2 = 3\phi^{'}/\pi^4, \quad \beta_3 = (2\phi/\pi^2) + (3\phi^{''}/\pi^4),\\
&\beta_4 = (4\phi^{'}/\pi^2) + (\phi^{'''}/\pi^4), \quad \beta_5 = \phi + (3\phi^{''}/\pi^2), \quad \beta_6 = \phi^{'} + (\phi^{'''}/\pi^2),\\
&\phi = [f(\theta)]^3, \quad f(\theta) = -4(r-1)\theta^2 + 4(r-1)\theta + 1.
\end{aligned}
$$

The variable coefficients in (80) involve sixth-order polynomials in θ. Six data sets, $\{7, 9, \cdots, 17\}$ Gauss-Lobatto points, are employed to study the convergence behaviour of the present method. Results concerning the fundamental frequency coefficient are shown in Table 7. They are compared well with those of [40] and [41]. It can be seen that the present method achieves a high level of accuracy using only a few grid points. For $r = 1.5$, at least 4 significant digits remain constant when $n \ge 13$.

5.1.2 A completely-free ring

In this case, a quarter of the ring structure is considered. It is convenient to introduce the dimensionless variable $\theta = \bar{\theta}/(\pi/2)$ here and the governing equation can be written as

$$\beta_1 v^{[6]} + \beta_2 v^{[5]} + \beta_3 v^{[4]} + \beta_4 v^{'''} + \beta_5 v^{''} + \beta_6 v^{'} - \Omega^2 \left(f v^{''} + f^{'} v^{'} - \pi^2 f v/4 \right) = 0, \quad (81)$$

with boundary conditions

$$
\begin{aligned}
v(0) &= v^{''}(0) = 0, \quad \phi^{'}(0) \left[v^{'}(0) + 4v^{'''}(0)/\pi^2 \right] + 4\phi(0) v^{[4]}(0)/\pi^2 = 0,\\
v(1) &= v^{''}(1) = 0, \quad \phi^{'}(1) \left[v^{'}(1) + 4v^{'''}(1)/\pi^2 \right] + 4\phi(1) v^{[4]}(1)/\pi^2 = 0,
\end{aligned}
$$

where

$$0 \leq \theta \leq 1,$$

$$\beta_1 = 16\phi/\pi^4, \quad \beta_2 = 48\phi^{'}/\pi^4, \quad \beta_3 = (8\phi/\pi^2) + (48\phi^{''}/\pi^4),$$

$$\beta_4 = (16\phi^{'}/\pi^2) + (16\phi^{'''}/\pi^4), \quad \beta_5 = \phi + (12\phi^{''}/\pi^2), \quad \beta_6 = \phi^{'} + (4\phi^{'''}/\pi^2),$$

$$\phi = [f(\theta)]^3, \quad f(\theta) = -(r-1)\theta^2 + 2(r-1)\theta + 1.$$

Convergence studies are conducted using five data sets of $\{5, 7, \cdots, 13\}$ Gauss-Lobatto points. Table 8 shows the fundamental frequencies obtained by the present method together with those of [40] and [41]. It can be seen that they are in good agreement. Highly accurate results are obtained with the present technique. For $r = 1.5$, at least 4 significant digits remain constant when $n \geq 9$.

5.2 Laminated composite plate

Laminated fibre composite plates have been extensively used in many fields of engineering such as aeronautics and space industries. Much research effort has been dedicated to improve the ability to predict the behaviour of these structures.

Using the first-order shear deformation theory, the equilibrium equations for moderately-thick laminated composite plates without membrane action can be written in the form [42]

$$A_{45}\Big(\frac{\partial^2 w}{\partial x \partial y} - \frac{\partial \psi_y}{\partial x}\Big) + A_{55}\Big(\frac{\partial^2 w}{\partial x^2} + \frac{\partial \psi_x}{\partial x}\Big) + A_{44}\Big(\frac{\partial^2 w}{\partial y^2} - \frac{\partial \psi_y}{\partial y}\Big) + A_{45}\Big(\frac{\partial^2 w}{\partial x \partial y} + \frac{\partial \psi_x}{\partial y}\Big) + q(x,y) = 0, \quad (82)$$

$$D_{16}\big(-\frac{\partial^2\psi_x}{\partial x^2}\big)+D_{26}\big(-\frac{\partial^2\psi_y}{\partial x\partial y}\big)+D_{66}\big(\frac{\partial^2\psi_x}{\partial x\partial y}-\frac{\partial^2\psi_y}{\partial x^2}\big)+$$
$$D_{12}\big(-\frac{\partial^2\psi_x}{\partial x\partial y}\big)+D_{22}\big(-\frac{\partial^2\psi_y}{\partial y^2}\big)+D_{26}\big(\frac{\partial^2\psi_x}{\partial y^2}-\frac{\partial^2\psi_y}{\partial x\partial y}\big)$$
$$=A_{44}\big(\frac{\partial w}{\partial y}-\psi_y\big)+A_{45}\big(\frac{\partial w}{\partial x}+\psi_x\big), \quad (83)$$

$$D_{16}\big(-\frac{\partial^2\psi_x}{\partial x\partial y}\big)+D_{26}\big(-\frac{\partial^2\psi_y}{\partial y^2}\big)+D_{66}\big(\frac{\partial^2\psi_x}{\partial y^2}-\frac{\partial^2\psi_y}{\partial x\partial y}\big)+$$
$$D_{11}\big(-\frac{\partial^2\psi_x}{\partial x^2}\big)+D_{12}\big(-\frac{\partial^2\psi_y}{\partial y\partial x}\big)+D_{16}\big(\frac{\partial^2\psi_x}{\partial y\partial x}-\frac{\partial^2\psi_y}{\partial x^2}\big)$$
$$=A_{45}\big(\frac{\partial w}{\partial y}-\psi_y\big)+A_{55}\big(\frac{\partial w}{\partial x}+\psi_x\big), \quad (84)$$

where w is the transverse displacement of a point situated in the middle plane, the xy plane; ψ_x and ψ_y are respectively the rotations of the transverse normal, i.e. in the z direction, with respect to the y and x axes; $q(x,y)$ is the transverse load; and

$$D_{ij}=\frac{1}{3}\sum_{k=1}^{n}(h_k^3-h_{k-1}^3)(\overline{Q_{ij}})_{(k)} \qquad i,j=1,2,6, \quad (85)$$

$$A_{ij}=\kappa\sum_{k=1}^{n}(h_k-h_{k-1})(\overline{C_{ij}})_{(k)}, \quad (86)$$

in which $\kappa=5/6$ is a shear correction factor, h is the thickness of the laminate, and $\overline{Q_{ij}}$ and $\overline{C_{ij}}$ represent the stiffness constants of a unidirectional orthotropic composite making an angle θ with the principal material x-axis. Equations (82)-(84) involve a large number of derivative terms, some of which are mixed partial derivatives.

The IRBFN method is applied to the static analysis of the bending behaviour of a simply-supported cross-ply laminate $a\times a$ with a cut-out concentric square hole $a/2\times a/2$. The composite plate consists of four layers $0^0/90^0/90^0/0^0$ under a uniform pressure q_0. The material properties are chosen to be

$E_1=25E_2,\ \nu_{12}=0.25,$

$G_{12}=G_{13}=0.5E_2,\ G_{23}=0.2E_2$

Different grids are employed for the study of grid convergence. A typical grid is plotted in Figure 5. Results are presented in dimensionless forms according to the following relations

$$w \rightarrow \frac{100 E_2 h^3}{q_0 a^4} w, \tag{87}$$

$$\{\sigma_{xx}, \sigma_{yy}, \tau_{xy}\} \rightarrow \frac{h^2}{q_0 a^2}\{\sigma_{xx}, \sigma_{yy}, \tau_{xy}\}, \tag{88}$$

$$\{\tau_{yz}, \tau_{xz}\} \rightarrow \frac{h}{q_0 a}\{\tau_{yz}, \tau_{xz}\}. \tag{89}$$

Good convergence is achieved as shown in Table 9. Figure 6 shows distributions of the displacement and in-plane stresses calculated at $z = h/2$.

5.3 Driven-cavity viscous flow

This problem is usually used as a model for the understanding of physical flows and for the testing of new numerical schemes in CFD. The lid-driven cavity flow possesses physically unrealistic characteristics (discontinuous velocity) at the edges of the lid. This leads to a rapid change in stress near those points, thereby making the numerical simulation difficult. In the context of Newtonian-fluid flow, Ghia, Ghia and Shin [43] have reported accurate solutions for a wide range of the Reynolds number using a multigrid finite-difference scheme with very dense grids. These results have often been cited in the literature for comparison purposes. Recently, by using the Chebyshev collocation technique, which exhibits exponential convergence/spectral accuracy, for the calculation of a regular part of the solution, and by using analytical formulae to obtain the singular part, Botella and Peyret [44] have provided benchmark spectral results on the flow at $Re = 1000$. It will be shown that the IRBFN results are in closer agreement with the spectral solutions than the finite-difference ones.

The lid velocity (U) and the side length of the cavity (L) are used as reference quantities. The dimensionless governing equations for unsteady two-dimensional incompressible flow of a Newtonian fluid in terms of stream function ψ and vorticity ω can be written as follows

$$\frac{\partial \omega}{\partial t} + \left(\frac{\partial \psi}{\partial y}\frac{\partial \omega}{\partial x} - \frac{\partial \psi}{\partial x}\frac{\partial \omega}{\partial y} \right) = \frac{1}{Re}\left(\frac{\partial^2 \omega}{\partial x^2} + \frac{\partial^2 \omega}{\partial y^2} \right), \tag{90}$$

$$\frac{\partial^2 \psi}{\partial x^2} + \frac{\partial^2 \psi}{\partial y^2} = -\omega, \tag{91}$$

where $Re = UL/\nu$ is the Reynolds number(ν: the kinematic viscosity). The vorticity and stream function are defined by

$$\omega = \frac{\partial v}{\partial x} - \frac{\partial u}{\partial y}, \tag{92}$$

$$\frac{\partial \psi}{\partial x} = -v, \quad \frac{\partial \psi}{\partial y} = u, \tag{93}$$

where u and v are two components of the velocity vector in the $x-$ and $y-$directions, respectively.

The lid slides toward the right at unit velocity, while the other walls remain stationary:

$$\psi = 0, \ \frac{\partial \psi}{\partial x} = 0, \quad \text{on} \quad x = 0 \text{ and } x = 1, \tag{94}$$

$$\psi = 0, \ \frac{\partial \psi}{\partial y} = 0, \quad \text{on} \quad y = 0, \tag{95}$$

$$\psi = 0, \ \frac{\partial \psi}{\partial y} = 1, \quad \text{on} \quad y = 1. \tag{96}$$

The boundary condition $\psi = 0$ along the boundaries can be used directly to solve (91) for the velocity field, while one needs to derive computational boundary conditions for the vorticity transport equation (90). Using (91) and the boundary condition $\psi = 0$, expressions for the vorticity on the boundaries are reduced to

$\omega = -\partial^2\psi/\partial n^2$ (n: the local coordinate normal to the wall). After expressing this normal second-order derivative as a linear combination of nodal first-order derivative values, imposition of the required boundary conditions $\partial\psi/\partial n$ is carried out. Finally, the remaining first derivative values are written in terms of nodal stream function values.

The stability of the lid-driven cavity flow was investigated by Poliashenko and Aidun [45]. For the case of a square cavity, it was reported that the point of bifurcation is $Re = 7763$, where the primary steady state becomes unstable. A range of the Re number, $\{0, 100, 400, 1000, 3200, 5000\}$, is considered here. The computed solution at the lower and nearest value of Re is taken to be the initial solution. The special case of $Re = 0$ starts from a fluid at rest. Ten uniform grids, namely $11 \times 11, 21 \times 21, \cdots, 101 \times 101$, are employed to study the convergence behaviour of the method. Time steps used are in the range of $0.005 - 0.5$. Steady-state solutions are presented in detail here, and they are compared with available data in the literature.

Results concerning the extrema of the velocity profiles along the vertical and horizontal centrelines ($Re = 100$ and $Re = 1000$) are summarized in Tables 10–11. The corresponding results obtained by the pseudospectral method [44], finite-difference method [43,46] and finite-volume method [47] are included for comparison. The IRBFN results are in better agreement with the spectral solutions than those predicted by the finite-difference and finite-volume methods.

Iso-vorticity lines of the flow for various Re numbers are shown in Figure 7. The vorticity-contour values chosen here are the same as those in [43,44], i.e. {-5, -4,-3,-2,-1,-0.5,0,0.5,1,2,3}. The plots look reasonable when compared to those of [43] and [44].

It is worth mentioning that although the present IRBFN method is global, it does

not require any special treatment for the singularity at the two corners. In contrast, when using the spectral collocation method, it is necessary to employ a subtraction technique to remove the leading part of the singularity.

6 Conclusion

In the present chapter, an overview of high-order integral collocation techniques using radial basis functions and Chebyshev polynomials is given. Three important features of these techniques are: (i) Using Cartesian grids to discretize the physical domain, (ii) Using point collocation to discretize the governing differential equation, and (iii) Employing high-order integrated approximants to represent the field variable, which result in effective numerical treatment schemes, particularly for handling irregular boundaries, high-order differential equations and large-scale domains. Several applications presented in this review illustrate the ability of the integral collocation approach to solve complicated engineering problems.

Acknowledgement

This work is supported by the Australian Research Council.

References

1. Roache, P.J. *Computational Fluid Dynamics*. Hermosa Publishers: Albuquerque, 1980.

2. Peyret, R. *Spectral Methods for Incompressible Viscous Flow*; Springer-Verlag: New York, 2002.

3. Zienkiewicz, O.C.; Taylor, R.L. *The Finite Element Method*; McGraw-Hill: London, 1991.

4. Brebbia, C.A.; Dominguez, J. *Boundary Elements An Introductory Course*; Computational Mechanics Publications: Southampton, 1992.

5. Mai-Duy, N.; Tran-Cong, T. Numerical solution of differential equations using multiquadric radial basis function networks. *Neural Networks*. 2001, 14, 185–199.

6. Mai-Duy, N.; Tran-Cong, T. Numerical solution of Navier-Stokes equations using multiquadric radial basis function networks. *International Journal for Numerical Methods in Fluids*. 2001, 37, 65–86.

7. Mai-Duy, N.; Tran-Cong, T. Mesh-free radial basis function network methods with domain decomposition for approximation of functions and numerical solution of Poisson's equations. *Engineering Analysis with Boundary Elements*. 2002, 26, 133–156.

8. Mai-Duy, N.; Tran-Cong, T. Approximation of function and its derivatives using radial basis function networks. *Applied Mathematical Modelling*. 2003, 27, 197–220.

9. Mai-Duy, N.; Tran-Cong, T. Indirect RBFN method with thin plate splines for numerical solution of differential equations. *Computer Modeling in Engineering & Sciences*. 2003, 4, 85–102.

10. Kansa, E.J.; Power, H.; Fasshauer, G.E.; Ling, L. A volumetric integral radial basis function method for time-dependent partial differential equations: I. Formulation. *Engineering Analysis with Boundary Elements*. 2004, 28, 1191–1206.

11. Ling, L.; Trummer, M.R. Multiquadric collocation method with integral formulation for boundary layer problems. *Computers & Mathematics with Applications*. 2004, 48(5–6), 927–941.

12. Mai-Duy, N. Indirect RBFN method with scattered points for numerical solution of PDEs. *Computer Modeling in Engineering & Sciences*. 2004, 6, 209–226.

13. Mai-Cao, L.; Tran-Cong, T. A meshless IRBFN-based method for transient problems. *Computer Modeling in Engineering & Sciences*. 2005, 7(2), 149–171.

14. Mai-Duy, N. Solving high order ordinary differential equations with radial basis function networks. *International Journal for Numerical Methods in Engineering*. 2005, 62, 824–852.

15. Mai-Duy, N.; Tanner, R.I. Solving high order partial differential equations with radial basis function networks. *International Journal for Numerical Methods in Engineering*. 2005, 63, 1636–1654.

16. Mai-Duy, N.; Tanner, R.I. Computing non-Newtonian fluid flow with radial basis function networks. *International Journal for Numerical Methods in Fluids*. 2005, 48, 1309–1336.

17. Mai-Duy, N.; Tran-Cong, T. An efficient indirect RBFN-based method for numerical solution of PDEs. *Numerical Methods for Partial Differential Equations*. 2005, 21, 770–790.

18. Deng, J. Structural reliability analysis for implicit performance function using radial basis function network. *International Journal of Solids and Structures*. 2006, 43(11–12), 3255–3291.

19. Ling, L.; Trummer, M.R. Adaptive multiquadric collocation for boundary layer problems. *Journal of Computational and Applied Mathematics*. 2006, 188(2), 265–282.

20. Mai-Duy, N. An effective spectral collocation method for the direct solution of high-order ODEs. *Communications in Numerical Methods in Engineering*. 2006, 22(6), 627–642.

21. Mai-Duy, N.; Tran-Cong, T. Solving biharmonic problems with scattered-point discretisation using indirect radial-basis-function networks. *Engineering Analysis with Boundary Elements*. 2006, 30(2), 77–87.

22. Sarra, S.A. Integrated multiquadric radial basis function approximation methods. *Computers & Mathematics with Applications*. 2006, 51(8), 1283–1296.

23. Le, P.; Mai-Duy, N.; Tran-Cong, T,; Baker, G. A numerical study of strain localization in elasto-thermo-viscoplastic materials using radial basis function networks. *Computers, Materials & Continua*. 2007, 5(2), 129–150.

24. Li, C.; Wu, X. Numerical solution of differential equations using Sinc method based on the interpolation of the highest derivatives. *Applied Mathematical Modelling*. 2007, 31(1), 1–9.

25. Mai-Duy, N.; Khennane, A.; Tran-Cong, T. Computation of laminated composite plates using integrated radial basis function networks. *Computers, Materials & Continua*. 2007, 5(1), 63–77.

26. Mai-Duy, N.; Mai-Cao, L.; Tran-Cong, T. Computation of transient viscous flows using indirect radial basis function networks. *Computer Modeling in Engineering & Sciences*. 2007, 18(1), 59–77.

27. Mai-Duy, N.; Tanner, R.I. A collocation method based on one-dimensional RBF interpolation scheme for solving PDEs. *International Journal of Numerical Methods for Heat & Fluid Flow*. 2007, 17(2), 165–186.

28. Mai-Duy, N.; Tanner, R.I. A spectral collocation method based on integrated Chebyshev polynomials for biharmonic boundary-value problems. *Journal of*

Computational and Applied Mathematics. 2007, 201(1), 30–47.

29. Shu, C.; Wu, Y.L. Integrated radial basis functions-based differential quadrature method and its performance. *International Journal for Numerical Methods in Fluids*. 2007, 53(6), 969–984.

30. Mai-Duy, N.; Tran-Cong, T. An efficient domain-decomposition pseudo-spectral method for solving elliptic differential equations. *Communications in Numerical Methods in Engineering*, in press

31. Mai-Duy, N.; Tran-Cong, T. A Cartesian-grid collocation method based on radial-basis-function networks for solving PDEs in irregular domains. *Numerical Methods for Partial Differential Equations*, in press

32. Mai-Duy, N.; See, H.; Tran-Cong, T. An integral-collocation-based fictitious domain technique for solving elliptic problems. Submitted.

33. Haykin, S. *Neural Networks: A Comprehensive Foundation*; Prentice-Hall: New Jersey, 1999.

34. Micchelli, C.A. Interpolation of scattered data: distance matrices and conditionally positive definite functions. *Constructive Approximation*. 1986, 2, 11–22.

35. Park, J.; Sandberg, I.W. Universal approximation using radial basis function networks. *Neural Computation*. 1991, 3, 246–257.

36. Cover, T.M. Geometrical and statistical properties of systems of linear inequalities with applications in pattern recognition. *IEEE Transactions on Electronic Computers*. 1965, EC-14, 326–334.

37. Madych, W.R.; Nelson, S.A. Multivariate interpolation and conditionally positive definite functions. *Approximation Theory and its Applications*. 1988, 4, 77–89.

38. Madych, W.R.; Nelson, S.A. Multivariate interpolation and conditionally positive definite functions, II. *Mathematics of Computation.* 1990, 54(189), 211-230.

39. Smith, B.F.; Bjorstad, P.E; Gropp, W.D. *Domain Decomposition Parallel Multilevel Methods for Elliptic Partial Differential Equations*; Cambridge University Press: New York, 1996.

40. Gutierrez, R.H.; Laura, P.A.A. Vibrations of non-uniform rings studied by means of the differential quadrature method. *Journal of Sound and Vibration.* 1995, 185(3), 507–513.

41. Wu, T.Y.; Liu, G.R. Application of generalized differential quadrature rule to sixth-order differential equations. *Communications in Numerical Methods in Engineering.* 2000, 16, 777–784.

42. Reddy, J.N. *Mechanics of laminated composite plates and shells. Theory and analysis*; CRC Press: Florida, 2004.

43. Ghia, U.; Ghia, K.N.; Shin, C.T. High-Re solutions for incompressible flow using the Navier-Stokes equations and a multigrid method. *Journal of Computational Physics.* 1982, 48, 387–411.

44. Botella, O.; Peyret, R. Benchmark spectral results on the lid-driven cavity flow. *Computers & Fluids.* 1998, 27(4), 421–433.

45. Poliashenko, M.; Aidun, C.K. A direct method for computation of simple bifurcations. *Journal of Computational Physics.* 1995, 121(2), 246–260.

46. Bruneau, C.-H.; Jouron, C. An efficient scheme for solving steady incompressible Navier-Stokes equations. *Journal of Computational Physics.* 1990, 89(2), 389–413.

47. Deng, G.B.; Piquet, J.; Queutey, P.; Visonneau, M. Incompressible flow calculations with a consistent physical interpolation finite volume approach. *Computers & Fluids*. 1994, 23(8), 1029–1047.

Table 1: Multiple boundary conditions: Condition numbers and errors by CSEs

$n_x \times n_y$	Differential Approach		Integral approach	
	$\text{cond}(\mathcal{A})$	$N_e(u)$	$\text{cond}(\mathcal{A})$	$N_e(u)$
6×6	4.4×10^2	1.23×10^{-1}	1.6×10^2	4.84×10^{-3}
8×8	3.6×10^3	5.94×10^{-3}	1.5×10^3	7.40×10^{-5}
10×10	2.0×10^4	2.10×10^{-4}	8.8×10^3	4.20×10^{-7}
12×12	9.2×10^4	4.46×10^{-6}	3.8×10^4	2.40×10^{-9}
14×14	3.4×10^5	6.52×10^{-8}	1.3×10^5	1.20×10^{-11}
16×16	1.1×10^6	7.05×10^{-10}	4.1×10^5	7.85×10^{-14}

Table 2: Multiple boundary conditions: Condition numbers and errors by RBFNs

$n_x \times n_y$	Differential Approach		Integral approach	
	cond($\mathcal{A}$)	$N_e(u)$	cond($\mathcal{A}$)	$N_e(u)$
7×7	6.3×10^5	1.40×10^{-1}	2.4×10^2	1.47×10^{-3}
11×11	3.4×10^6	1.22×10^{-1}	2.4×10^3	1.61×10^{-4}
17×17	1.8×10^7	1.46×10^{-1}	1.8×10^4	4.03×10^{-5}
21×21	4.4×10^7	1.82×10^{-1}	4.5×10^4	2.44×10^{-5}
27×27	1.2×10^8	2.33×10^{-1}	1.3×10^5	1.41×10^{-5}
31×31	2.1×10^8	2.64×10^{-1}	2.3×10^5	1.05×10^{-5}
37×37	4.4×10^8	3.05×10^{-1}	4.9×10^5	7.35×10^{-6}
41×41	6.7×10^8	3.30×10^{-1}	7.5×10^5	5.95×10^{-6}
47×47	1.1×10^9	3.63×10^{-1}	1.3×10^6	4.50×10^{-6}

Table 3: Non-rectangular boundaries: Condition numbers and errors by ICSEs

$n_x \times n_y$	$\mathrm{cond}(\mathcal{A})$	$N_e(u)$
6×6	3.9×10^2	3.58×10^{-3}
8×8	1.1×10^3	8.08×10^{-5}
10×10	5.3×10^3	6.36×10^{-7}
12×12	2.1×10^4	7.27×10^{-9}
14×14	1.0×10^5	4.49×10^{-11}
16×16	4.8×10^5	3.21×10^{-13}
18×18	2.0×10^6	4.85×10^{-14}
20×20	8.7×10^6	3.26×10^{-14}

Table 4: Non-rectangular boundaries: Condition numbers and errors by IRBFNs

$n_x \times n_y$	$\mathrm{cond}(\mathcal{A})$	$N_e(u)$
4×4	3.2×10^{0}	2.90×10^{-1}
9×9	4.1×10^{1}	1.11×10^{-3}
14×14	2.6×10^{2}	3.63×10^{-4}
19×19	2.6×10^{2}	1.36×10^{-4}
24×24	7.0×10^{2}	6.67×10^{-5}
29×29	6.5×10^{2}	4.36×10^{-5}
34×34	1.3×10^{3}	1.33×10^{-5}
39×39	2.2×10^{3}	7.87×10^{-6}
44×44	2.1×10^{3}	5.35×10^{-6}
49×49	3.2×10^{3}	4.07×10^{-6}

Table 5: Domain decomposition: Errors by CSEs

n	$N_e(u)$	
(Points/subdomain)	Differential approach	Integral approach
3	6.63×10^{-2}	2.55×10^{-3}
5	6.12×10^{-4}	4.47×10^{-6}
7	2.15×10^{-6}	2.16×10^{-9}
9	3.94×10^{-9}	1.34×10^{-12}
11	4.41×10^{-12}	8.04×10^{-16}
13	3.16×10^{-15}	5.40×10^{-16}

Table 6: Domain decomposition: Errors by RBFNs

n	$N_e(u)$	
(Points/subdomain)	Differential approach	Integral approach
11	4.34×10^{-1}	4.92×10^{-4}
21	4.25×10^{-1}	1.23×10^{-4}
31	4.22×10^{-1}	5.53×10^{-5}
41	4.21×10^{-1}	3.12×10^{-5}
51	4.20×10^{-1}	2.00×10^{-5}
61	4.20×10^{-1}	1.39×10^{-5}
71	4.20×10^{-1}	1.02×10^{-5}
81	4.19×10^{-1}	7.83×10^{-6}
91	4.19×10^{-1}	6.19×10^{-6}
101	4.19×10^{-1}	5.02×10^{-6}

Table 7: Free vibration of a non-uniform ring with constraints: fundamental frequencies. It is noted that DQ and RR stand for the differential quadrature and Rayleigh-Ritz methods, respectively.

	ICSEs						DQ	RR
r	7	9	11	13	15	17	[41]	[40]
1.0	2.2659	2.2667	2.2667	2.2667	2.2667	2.2667	2.2667	2.274
1.1	2.4134	2.4137	2.4137	2.4137	2.4137	2.4137	2.4137	2.416
1.2	2.5531	2.5569	2.5568	2.5568	2.5568	2.5568	2.5568	2.557
1.3	2.6690	2.6975	2.6966	2.6966	2.6966	2.6966	2.6966	2.697
1.4	2.7086	2.8387	2.8334	2.8334	2.8334	2.8334	2.8335	2.834
1.5	2.5572	2.9886	2.9673	2.9677	2.9677	2.9677	2.9678	2.970

Table 8: Free vibration of a non-uniform ring without constraints: fundamental frequencies. It is noted that DQ and RR stand for the differential quadrature and Rayleigh-Ritz methods, respectively.

	ICSEs					DQ	RR
r	5	7	9	11	13	[41]	[40]
1.0	2.6822	2.6833	2.6833	2.6833	2.6833	2.6833	2.687
1.1	2.8450	2.8452	2.8452	2.8452	2.8452	2.8452	2.846
1.2	3.0063	3.0062	3.0062	3.0062	3.0062	3.0062	3.006
1.3	3.1672	3.1665	3.1665	3.1665	3.1665	3.1665	3.167
1.4	3.3279	3.3262	3.3263	3.3263	3.3263	3.3263	3.326
1.5	3.4886	3.4857	3.4858	3.4858	3.4858	3.4858	3.486

Table 9: Laminated composite plate: Displacement and stresses.

Density	$w(a/2, a/8)$	$\sigma_{xx}(a/2, a/8, h/2)$	$\sigma_{yy}(a/2, a/8, h/2)$	$\tau_{xy}(a/2, a/8, h/2)$	$\tau_{yz}(a/2, 0, 0)$	$\tau_{xz}(0, a/2, 0)$
17×17	2.9590×10^{-2}	8.0824×10^{-4}	3.7160×10^{-3}	1.6625×10^{-8}	-4.3448×10^{-2}	-4.0660×10^{-2}
25×25	2.9900×10^{-2}	1.3515×10^{-3}	3.7761×10^{-3}	1.5205×10^{-9}	2.1391×10^{-1}	1.0193×10^{-1}
33×33	3.0060×10^{-2}	1.2745×10^{-3}	3.9142×10^{-3}	1.6929×10^{-10}	2.9333×10^{-1}	1.4319×10^{-1}
41×41	3.0148×10^{-2}	1.1473×10^{-3}	3.9290×10^{-3}	1.9078×10^{-11}	3.1695×10^{-1}	1.5514×10^{-1}
49×49	3.0199×10^{-2}	1.0453×10^{-3}	3.9460×10^{-3}	-5.5379×10^{-13}	3.2419×10^{-1}	1.5870×10^{-1}
57×57	3.0232×10^{-2}	9.6820×10^{-4}	3.9525×10^{-3}	1.7980×10^{-11}	3.2681×10^{-1}	1.5993×10^{-1}
65×65	3.0253×10^{-2}	9.1134×10^{-4}	3.9576×10^{-3}	1.4088×10^{-11}	3.2804×10^{-1}	1.6048×10^{-1}

Table 10: Lid-driven cavity flow, $Re = 100$: Extrema of the vertical and horizontal velocity profiles through the centre of the cavity.

Method	Density	u_{min}(error %)	y	v_{2max}(error %)	x	v_{min}(error %)	x
Present	11×11	-0.18388(14.091)	0.484	0.14175(21.061)	0.242	-0.20870(17.770)	0.814
	21×21	-0.21085(1.490)	0.464	0.17450(2.823)	0.239	-0.24734(2.545)	0.808
	31×31	-0.21367(0.173)	0.459	0.17895(0.345)	0.237	-0.25278(0.402)	0.810
	41×41	-0.21408(0.019)	0.458	0.17960(0.017)	0.237	-0.25368(0.047)	0.810
FVM [47]	64×64	-0.21315(0.416)	—	0.17896(0.340)	—	-0.25339(0.162)	—
FDM($\psi - \omega$) [43]	129×129	-0.21090(1.467)	0.453	0.17527(2.395)	0.234	-0.24533(3.337)	0.805
FDM($\mathbf{u} - p$) [46]	129×129	-0.2106 (1.607)	0.453	0.1786 (0.540)	0.234	-0.2521 (0.670)	0.813
Benchmark [44]		-0.21404	0.458	0.17957	0.237	-0.25380	0.810

Table 11: Lid-driven cavity flow, $Re = 1000$: Extrema of the vertical and horizontal velocity profiles through the centre of the cavity. It is noted that cpi and stagg stand for consistent physical interpolation and staggered, respectively.

Method	Density	u_{min}(error %)	y	v_{max}(error %)	x	v_{min}(error %)	x
Present	11×11	-0.16933(56.422)	0.244	0.14892(60.492)	0.218	-0.20926(60.298)	0.906
	21×21	-0.28334(27.081)	0.254	0.25166(33.236)	0.185	-0.35962(31.771)	0.875
	31×31	-0.33588(13.560)	0.192	0.32263(14.408)	0.167	-0.46097(12.543)	0.891
	41×41	-0.36667(5.636)	0.177	0.35368(6.171)	0.163	-0.49844(5.434)	0.903
	51×51	-0.37859(2.568)	0.174	0.36588(2.934)	0.161	-0.51356(2.565)	0.907
	61×61	-0.38300(1.434)	0.174	0.37060(1.682)	0.160	-0.51939(1.459)	0.908
	71×71	-0.38496(0.929)	0.173	0.37279(1.101)	0.159	-0.52199(0.966)	0.908
	81×81	-0.38603(0.654)	0.173	0.37403(0.772)	0.159	-0.52344(0.691)	0.909
	91×91	-0.38671(0.479)	0.173	0.37482(0.562)	0.159	-0.52436(0.516)	0.909
	101×101	-0.38717(0.360)	0.172	0.37536(0.419)	0.158	-0.52499(0.397)	0.909
FVM,stagg.	128×128	-0.38050(2.077)	—	0.36884(2.149)	—	-0.51727(1.861)	—
FVM,cpi.	128×128	-0.38511(0.890)	—	0.37369(0.862)	—	-0.52280(0.812)	—
[47]							
FDM($\psi - \omega$)	129×129	-0.38289(1.462)	0.172	0.37095(1.589)	0.156	-0.51550(2.197)	0.906
[43]							
FDM($\mathbf{u} - p$)	256×256	-0.3764 (3.132)	0.160	0.3665 (2.770)	0.152	-0.5208 (1.192)	0.910
[46]							
Benchmark		-0.38857	0.172	0.37694	0.158	-0.52708	0.909
[44]							

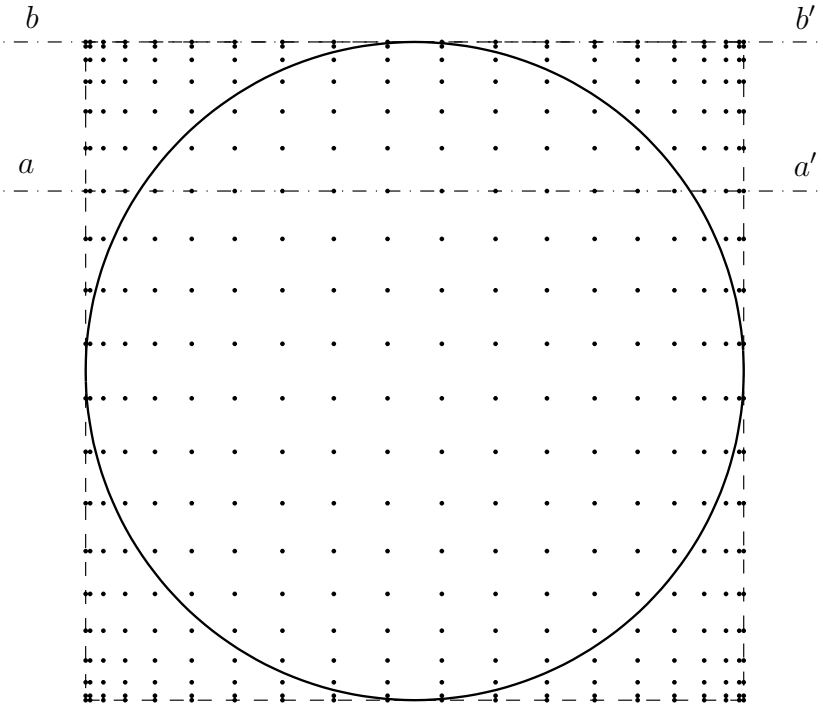

Figure 1: ICSE discretization.

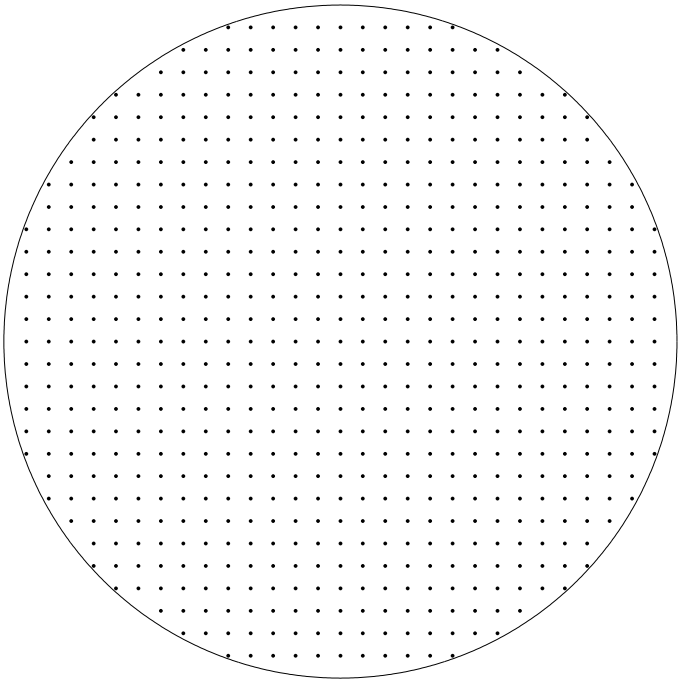

Figure 2: IRBFN discretization.

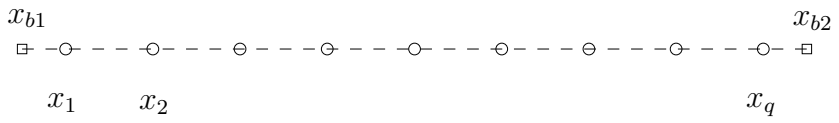

Figure 3: Points on a grid line in the IRBFN discretization scheme consist of interior points x_i ($\circ$) and boundary points x_{bi} ($\square$).

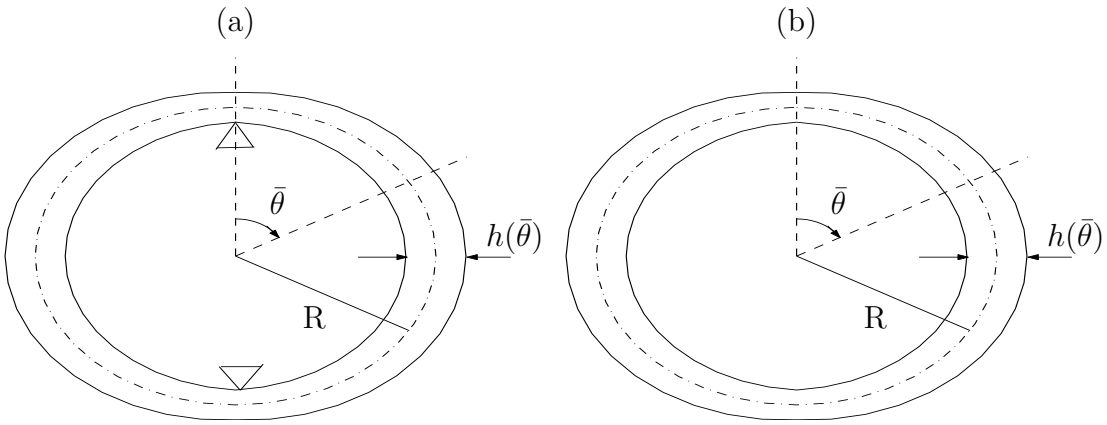

Figure 4: Free vibrations of rings: (a) with constraints and (b) without constraints.

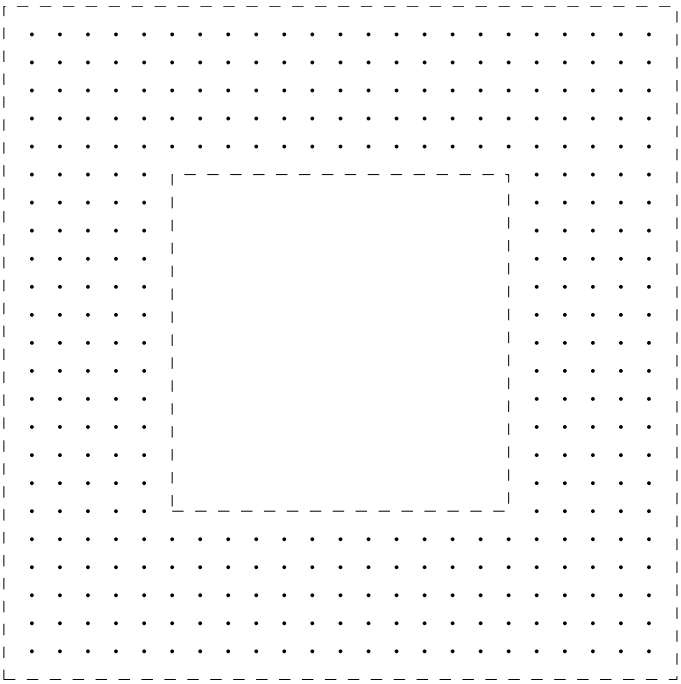

Figure 5: Laminated composite plate: a typical IRBFN discretization.

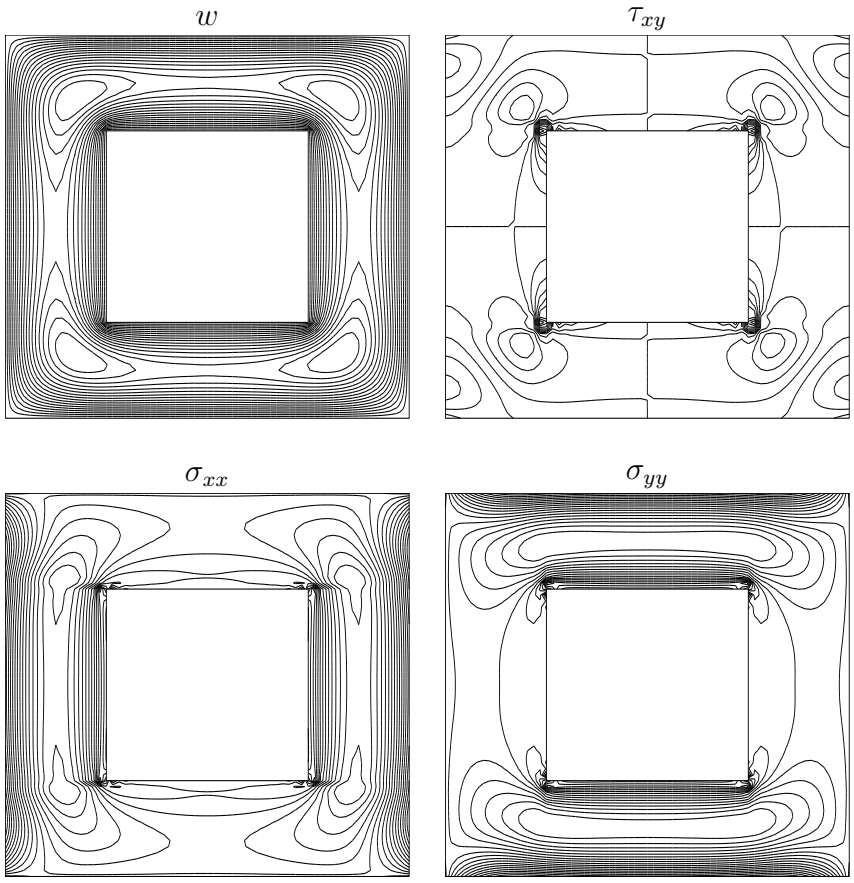

Figure 6: Laminated composite plate: Displacement and in-plane stresses at $z = h/2$.

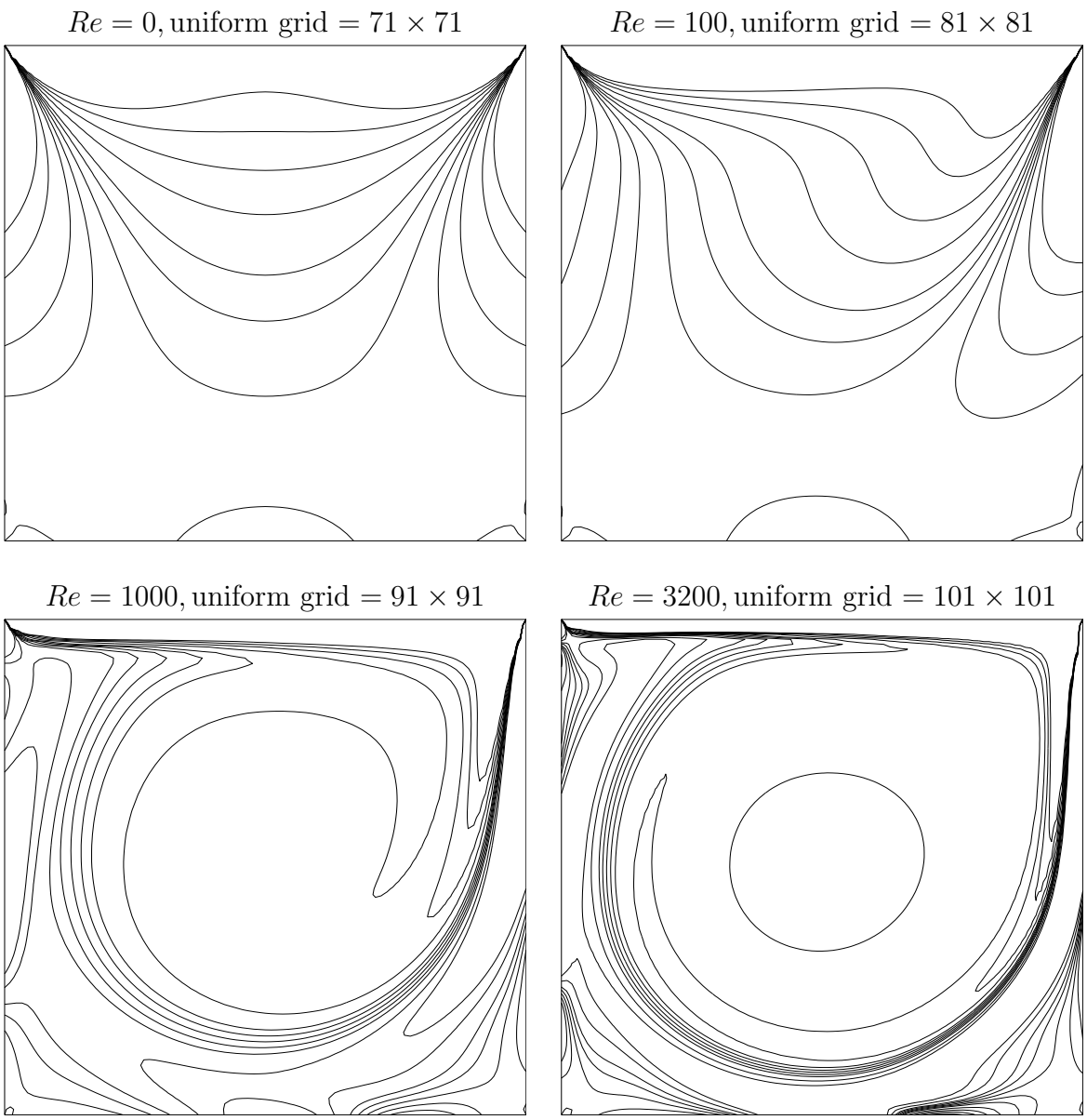

Figure 7: Lid-driven cavity flow: Iso-vorticity lines of the flow for various Re numbers.